
Simulating Ising and Potts models at critical and cold temperatures using auxiliary Gaussian variables

Charles C. Margossian
 Department of Statistics,
 Columbia University
 charles.margossian@columbia.edu

Sumit Mukherjee
 Department of Statistics,
 Columbia University
 sm3949@columbia.edu

Abstract

Ising and Potts models are an important class of discrete probability distributions which originated from Statistical Physics and since then have found applications in several disciplines. Simulation from these models is a well known challenging problem. In this paper, we propose a class of MCMC algorithms to simulate from both Ising and Potts models, by using auxiliary Gaussian random variables. Our algorithms apply to coupling matrices with both positive and negative entries, thus including Spin Glass models such as the SK and Hopfield model. In contrast to existing methods of a similar flavor, our algorithm can take advantage of the low-rank structure of the coupling matrix, and scales linearly with the number of states in a Potts model. We compare our proposed algorithm to existing state of the art algorithms, such as the Swendsen-Wang and Wolff algorithms for Ising and Potts models on graphs, and the Heat Bath for Spin Glass models. Our comparison takes into account a wide range of coupling matrices and temperature regimes, focusing in particular on behavior at or below the critical temperature. For cold systems, augmenting our algorithm with a tempering scheme yields significant improvements.

1 Introduction

The Ising model is a probability distribution on the space of binary vectors of size n , whose components are allowed to take two values, often termed *spins*, which are traditionally taken to $\{0, 1\}$ or $\{-1, 1\}$. The Ising model was first introduced in Statistical Physics [Ising, 1925] to study ferromagnetism. The Potts model [Potts, 1952] generalizes the Ising model

to $q \geq 2$ states, where the states can be taken to be $[q] := \{1, 2, \dots, q\}$ without loss of generality. With this choice, the Potts model is given by the following probability mass function on $[q]^n$:

$$\mathbb{P}(\mathbf{X} = \mathbf{x}) = \frac{\exp(\frac{\beta}{2} \sum_{i,j=1}^n A_n(i,j) 1\{x_i = x_j\})}{Z(\beta, A_n)}. \quad (1)$$

Here $\beta > 0$ is the inverse temperature parameter; the coupling matrix A_n is a symmetric matrix which controls the dependence between the components of \mathbf{X} , and $Z(\beta, A_n)$ is the normalizing constant, also termed the partition function. We assume that the diagonal entries of A_n equal 0, noting that this does not have any impact on the model (1). Since their inception, both the Ising and Potts models have found applications in a wide range of disciplines, ranging from Image Processing, Protein Folding, Neuroscience, and Social Sciences. One of the main reasons for the popularity of these models is that they are perhaps the simplest models which exhibit non-trivial dependence across their components.

1.1 Examples of Ising and Potts models

In the particular case where the coupling matrix is a scaled adjacency matrix of a graph G_n , the Ising/Potts model is a discrete Markov random field. Of particular interest are the Ising/Potts models on the following graphs:

- **Curie-Weiss model.** Here G_n is the complete graph, and $A_n(i, j) = \frac{1}{n} \delta_{i \neq j}$;
- **Ising model on the integer lattice.** Here A_n is the adjacency matrix of a sub-cube of the integer lattice $[1, n^{1/d}]^d$ (assume $n^{1/d}$ is an integer for simplicity);
- **Ising model on random graphs.** Here $A_n = \frac{1}{\bar{d}(G_n)} G_n$, where $\bar{d}(G_n)$ is the average degree of

the graph G_n , and G_n is random (e.g. Erdős-Rényi random graphs, Random regular graphs, graphons).

On the other hand, if the coupling matrix A_n is allowed to take both positive and negative real entries, then the corresponding Ising model is typically referred to as Spin Glass in the literature. The two most commonly studied examples of Spin Glass models are the following:

- **Sherrington Kirkpatrick model.** Here $\{A_n(i, j)\}_{1 \leq i < j \leq n} \stackrel{i.i.d.}{\sim} N(0, 1/n)$;
- **Hopfield model.** Here $A_n = \frac{1}{\max(n, d)} \eta' \eta$, where η is a $d \times n$ matrix of i.i.d. Rademacher random variables.

In all these examples the scaling of A_n is done to ensure that the log partition function scales in a non-trivial manner for large n . To discuss the scaling choices, we introduce the following standard asymptotic notations:

Definition 1 Suppose $\{a_n\}_{n \geq 1}$ and $\{b_n\}_{n \geq 1}$ are two positive real sequences. We will say

$$\begin{aligned}
 a_n &= o(b_n) \text{ or } a_n \ll b_n \text{ if } \lim_{n \rightarrow \infty} \frac{a_n}{b_n} = 0, \\
 a_n &= O(b_n) \text{ if } \limsup_{n \rightarrow \infty} \frac{a_n}{b_n} < \infty, \\
 a_n &= \Theta(b_n) \text{ if } a_n = O(b_n) \text{ and } b_n = O(a_n).
 \end{aligned}$$

Throughout the paper, all scalings of A_n are chosen such that $\log Z(\beta, A_n) = \Theta(n)$, i.e. the log partition function scales linearly in n as $n \rightarrow \infty$. This choice of scaling ensures that the model has a non-trivial phase transition in the parameter β , which is of interest in Statistical Physics and Probability [cf. Basak and Mukherjee, 2017, and references therein]. One sufficient condition for $\log Z(\beta, A_n) = \Theta(n)$ is $\lambda_{\max} = \Theta(1)$, where λ_{\max} denotes the largest eigenvalue of A_n . Except for very special cases and small systems, we cannot compute the normalizing constant $Z(\beta, A_n)$ in (1). This means various quantities of interest are intractable, including the partition function and other derived quantities, and need to be estimated, for instance, using Markov chains Monte Carlo (MCMC) methods.

1.2 Existing methods

Drawing samples from Ising/Potts models can be a challenging task, with the performance and even applicability of existing methods depending on the type

of coupling matrix A_n and the system’s “temperature” β^{-1} . Perhaps the most popular methods in Physics are auxiliary cluster algorithms, notably the Swendsen-Wang and Wolff algorithms [Swendsen and Wang, 1987, Wolff, 1989], which continue to be used for high-precision Monte Carlo estimation [e.g. Ferrenberg et al., 2018]. These methods are particularly well suited for studying systems at critical and cold temperatures, however they only apply to Ising/Potts models defined on graphs. For Spin Glass models, a well-studied method is Heat Bath, also termed the sequential Gibbs, [e.g Neal, 1993], often augmented with a tempering scheme when studying cold systems [e.g. Swendsen and Wang, 1986, Hukushima et al., 1998, Katzgraber et al., 2001, Yucesoy, 2013].

A relatively recent approach is to introduce an auxiliary multivariate Gaussian variable, \mathbf{Z} , and construct MCMC over the augmented space, (\mathbf{X}, \mathbf{Z}) , to sample from binary random Markov fields, a special class of Ising models where A_n is a (scaled) adjacency matrix [Martens and Sutskever, 2010, Zhang et al., 2012]. Our work generalizes this approach to Potts models. Martens and Sutskever [2010] note that their method extends to the non-binary case, by introducing an nq -multivariate normal, but this results in a Gibbs sampler with computational complexity $O(n^3 q^3 + mn^2 q^2)$, where m is the number of sampling iterations. The algorithm we propose achieves $O(n^3 + mn^2 q)$ complexity, and a suitable low-rank approximation can further reduce this cost. We also note that in their study Martens and Sutskever [2010] found the Auxiliary Gaussian Gibbs sampler did not outperform the Heat Bath, which stands in contrast to our results. By examining a broad range of coupling matrices and temperatures, we identify the model regimes where using an auxiliary Gaussian works best and where it fails.

Rather than use a block Gibbs sampler, it is possible to sample over the marginal space of \mathbf{Z} using a gradient-based algorithm [Zhang et al., 2012]. We will see that our method is amiable to this scheme, however this paper focuses on a block Gibbs sampler which is more straightforward to analyze and implement. There also exist general purpose gradient-based algorithms which attempt a continuous relaxation of discrete systems [e.g. Grathwohl et al., 2021] but we expect these do not perform as well as more specialized algorithms for Ising/Potts models.

2 Choices of Auxiliary Gaussian

2.1 Auxiliary Gaussian for Potts

Given a vector $\mathbf{x} = (x_1, \dots, x_n) \in [q]^n$, for every $\ell \in [q]$ define a vector $\mathbf{y}_\ell := (1\{x_1 = \ell\}, \dots, 1\{x_n = \ell\})' \in \mathbb{R}^n$. In other words, the i^{th} element of \mathbf{y}_ℓ is 1 if $x_i = \ell$, and 0 otherwise. This sets up a one-to-one map between \mathbf{x} and $(\mathbf{y}_1, \dots, \mathbf{y}_q)$. Then we have

$$\frac{1}{2} \sum_{i,j=1}^n A_n(i, j) 1\{x_i = x_j\} = \frac{1}{2} \sum_{\ell=1}^q \mathbf{y}'_\ell A_n \mathbf{y}_\ell.$$

The term $\frac{1}{2} \mathbf{y}'_\ell A_n \mathbf{y}_\ell$ looks like the log moment generating function of a multivariate Gaussian, except that the matrix A_n is not non-negative definite, as the diagonal entries of A_n equal 0. Let λ_{\min} be the smallest eigenvalue of A_n . Since changing the diagonal entries of A_n does not impact the Potts model, we can replace A_n by $A_n + \lambda I_n$ where $\lambda > |\lambda_{\min}|$, and $A_n + \lambda I_n$ is positive definite. To check that the model (1) does not change under this transformation, note that

$$\begin{aligned} & \sum_{\ell=1}^q \mathbf{y}'_\ell (A_n + \lambda I_n) \mathbf{y}_\ell - \sum_{\ell=1}^q \mathbf{y}'_\ell A_n \mathbf{y}_\ell \\ &= \lambda \sum_{\ell=1}^q \mathbf{y}'_\ell \mathbf{y}_\ell = \lambda \sum_{\ell=1}^q \sum_{i=1}^n 1\{x_i = \ell\} = n\lambda, \end{aligned}$$

where the last equality follows from the fact $\sum_{\ell=1}^q 1\{x_i = \ell\} = 1$ for each $i \in [n]$. Setting $B_n := \beta(A_n + \lambda I_n)$, the marginal probability mass function of \mathbf{X} can be written as

$$\mathbb{P}(\mathbf{X} = \mathbf{x}) = \frac{\exp\left(\frac{1}{2} \sum_{\ell=1}^q \mathbf{y}'_\ell B_n \mathbf{y}_\ell\right)}{Z(\beta, B_n)}. \quad (2)$$

Given $\mathbf{X} = \mathbf{x}$, let $\mathbf{Z}_1, \dots, \mathbf{Z}_q$ be mutually independent Gaussian random vectors with

$$\mathbf{Z}_\ell \sim N(\mathbf{y}_\ell, B_n^{-1}). \quad (3)$$

Then one can check that given $\mathbf{Z} := (\mathbf{Z}_1, \dots, \mathbf{Z}_q)$ the random variables (X_1, \dots, X_n) are mutually independent, with

$$\mathbb{P}(X_i = \ell \mid \mathbf{Z}) = \frac{\exp\left(\sum_{j=1}^n B_n(i, j) z_\ell(j)\right)}{\sum_{a=1}^q \exp\left(\sum_{j=1}^n B_n(i, j) z_a(j)\right)}. \quad (4)$$

Also, the marginal density of \mathbf{Z} is proportional to

$$\exp\left(-\frac{1}{2} \sum_{\ell=1}^q \mathbf{z}'_\ell B_n \mathbf{z}_\ell\right) \prod_{i=1}^n \left(\sum_{\ell=1}^q \exp\left(\sum_{j=1}^n B_n(i, j) z_\ell(j)\right)\right). \quad (5)$$

The proofs of both (4) and (5) are in the Supplement.

2.2 Sampling based on an Auxiliary Gaussian

By iterating between (3) and (4), we obtain a block Gibbs sampling algorithm, where one alternates between sampling $(\mathbf{Z} \mid \mathbf{X})$ and $(\mathbf{X} \mid \mathbf{Z})$. (Algorithm 1).

Algorithm 1 Block Gibbs sampling for Potts model to compute m approximate samples

- 1: **input:** initial state, $\mathbf{x}^{(0)}$, coupling matrix, A_n , inverse temperature, β , number of iterations, m .
 - 2: $\lambda > |\lambda_{\min}(A_n)|$, where $\lambda_{\min}(A_n)$ = smallest eigenvalue of A_n .
 - 3: $B_n = \beta(A_n + \lambda I_n)$.
 - 4: $L_n = \text{Cholesky-decompose}([B_n]^{-1})$.
 - 5: **for** i in $1 : m$ **do**:
 - 6: **for** ℓ in $1 : q$ **do**:
 - 7: $\mathbf{y}_\ell = \left(1\{x_1^{(i-1)} = \ell\}, \dots, 1\{x_n^{(i-1)} = \ell\}\right)$.
 - 8: $\mathbf{z}_n^* \sim \text{Normal}(0, I_n)$.
 - 9: $\mathbf{z}_\ell = L_n \mathbf{z}_n^* + \mathbf{y}_\ell$.
 - 10: **end for**.
 - 11: $P_n = B_n[\mathbf{z}_1, \dots, \mathbf{z}_q]$.
 - 12: **for** j in $1 : n$ **do**:
 - 13: $\mathbf{p}_q = (\exp(P_n(j, \ell)), \ell \in [q])$.
 - 14: $\mathbf{x}_j^{(i)} \sim \text{Categorical}(\mathbf{p}_q / \sum_{a=1}^q p_q(a))$.
 - 15: **end for**.
 - 16: **return:** $\mathbf{x}^{(1)}, \mathbf{x}^{(2)}, \dots, \mathbf{x}^{(m)}$.
 - 17: **end for**
-

A key observation is that the covariance for the \mathbf{Z}_ℓ 's remains unchanged between sampling iterations. Hence we only need to perform the Cholesky decomposition and inversion of $B_n = \beta A_n + \lambda I_n$ once. This is an expensive operation with complexity $\mathcal{O}(n^3)$. Within each iteration, the cost is dominated by $2q$ matrix-vector multiplications, each with cost $\mathcal{O}(n^2)$. The complexity of the algorithm is therefore $\mathcal{O}(n^3 + mn^2q)$. Provided $n \ll m$, the cost of the initial operation is marginal.

2.3 Low-rank Auxiliary Gaussian

For certain models, the coupling matrix B_n may be low-rank, either exactly or approximately. In this case, it is reasonable to believe that we don't have to work with n -dimensional Gaussian vectors, but instead with a k -dimensional Gaussian vector, where $k = \text{rank}(B_n)$. In fact, such algorithms have already been explored in the setting of Ising models for the complete graph [Mukherjee et al., 2018], where $A_n = \frac{1}{n} \mathbf{1}\mathbf{1}' - \frac{1}{n} I_n$ has eigenvalues $(1 - \frac{1}{n}, -\frac{1}{n}, \dots, -\frac{1}{n})$, where the multiplicity of the eigenvalue $-\frac{1}{n}$ is $n-1$. Even though $\text{rank}(A_n) = n$ in a strict sense, we can add $-\frac{1}{n} I_n$ to A_n to get the matrix $\frac{1}{n} \mathbf{1}\mathbf{1}'$, which has eigenvalues $(1, 0, \dots, 0)$, and rank 1. A similar approach was successful in analyzing the Ising model of a regular graph with degree $\propto \sqrt{n}$ [Mukherjee and Xu, 2021], where $\text{rank}(A_n) \propto \sqrt{n}$.

To propose a general version of the low-rank algorithm, let $B_n = \beta(A_n + |\lambda_{\min}|I_n)$. Note it is sufficient to augment the diagonal elements with $|\lambda_{\min}|$, rather than $\lambda > |\lambda_{\min}|$. Let $\sum_{i=1}^n \mu_i \mathbf{p}_i \mathbf{p}_i'$ denote the spectral expansion of B_n , where (μ_1, \dots, μ_n) are non-negative, and arranged in decreasing order, and $\mathbf{p}_i \in \mathbb{R}^n$ is the eigenvector corresponding to eigenvalue μ_i . Fixing $\varepsilon > 0$, we introduce the low-rank approximation

$$\tilde{B}_n = \sum_{i: \mu_i > \varepsilon} \mu_i \mathbf{p}_i \mathbf{p}_i'.$$

In other words, we treat the eigenvalues below ε as 0. Let $k \leq n$ denote the rank of \tilde{B}_n , i.e. $k := \sum_{i=1}^n \mathbf{1}\{\mu_i > \varepsilon\}$. Let \mathbb{Q} be the Potts model with B_n replaced by \tilde{B}_n , i.e.

$$\mathbb{Q}(\mathbf{X} = \mathbf{x}) = \frac{\exp(\frac{1}{2} \sum_{i,j=1}^n \tilde{B}_n(i,j) \mathbf{1}\{x_i = x_j\})}{Z(\beta, \tilde{B}_n)}. \quad (6)$$

The hamiltonian of the probability measure \mathbb{Q} can be written as

$$\frac{1}{2} \sum_{\ell=1}^q \mathbf{y}'_{\ell} \tilde{B}_n \mathbf{y}_{\ell} = \frac{1}{2} \sum_{\ell=1}^q \sum_{j=1}^k \mu_j (\mathbf{p}'_j \mathbf{y}_{\ell})^2. \quad (7)$$

This representation motivates the following new auxiliary variable. Given $\mathbf{X} = \mathbf{x}$, let $\mathbf{Z} := \{Z_{\ell}(j)\}_{\ell \in [q], j \in [k]}$ be kq mutually independent Gaussians with

$$Z_{\ell}(j) \sim \text{Normal}(\mathbf{p}'_j \mathbf{y}_{\ell}, 1/\mu_j). \quad (8)$$

Then the conditional distribution of \mathbf{X} given \mathbf{Z} is given by

$$\mathbb{P}(X_i = \ell \mid \mathbf{Z}) = \frac{\exp\left(\sum_{j=1}^k \mu_j z_{\ell}(j) p_j(i)\right)}{\sum_{a=1}^q \exp\left(\sum_{j=1}^k \mu_j z_a(j) p_j(i)\right)}, \quad (9)$$

which is straightforward to sample from. Also, the marginal density of \mathbf{Z} has a similar low-rank structure, and is proportional to

$$\exp\left(-\frac{1}{2} \sum_{\ell=1}^q \sum_{j=1}^k \mu_j z_{\ell}(j)^2\right) \prod_{i=1}^n \left(\sum_{\ell=1}^q \exp\left(\sum_{j=1}^k \mu_j z_{\ell}(j) p_j(i)\right)\right) \quad (10)$$

The proof of both (9) and (10) are given in the Supplementary Material.

By iterating between the steps (8) and (9), we again have a block Gibbs sampler. We no longer need to do an inversion and Cholesky decomposition, but we do one Eigen decomposition instead, which incurs the same complexity $\mathcal{O}(n^3)$. The cost per iteration is dominated by (i) calculating the mean of each univariate normal, that is doing qk inner-products of n -vectors,

and (ii) calculating the probability of sampling each state for each particle, which is qn inner-products of k -vectors. The resulting Gibbs sampler has complexity $\mathcal{O}(n^3 + mqnk)$. This is an improvement over the previously obtained complexity $\mathcal{O}(n^3 + mqn^2)$. In particular the improvement is significant when $m \gg n \gg k$.

Remark 2 Another MCMC algorithm arises out of our analysis, using (5) (or (10)), which gives the unnormalized marginal density of the matrix \mathbf{Z} . Since \mathbf{Z} is continuous, we can use gradient-based algorithms to simulate \mathbf{Z} , and subsequently sample \mathbf{X} from (4) (or (9)). A low-rank approximation of A_n will give a low-rank version of the density of \mathbf{Z} , which also improves the computation of gradient-based algorithms.

2.4 Low-rank approximation error

It is natural to guess that the low-rank Auxiliary Gaussian method outperforms the usual Auxiliary Gaussian Method when the matrix A_n is approximately of low-rank. A more refined question is whether we can provide rigorous bounds on the error in this approximate algorithm, which allows the user to choose the tuning parameter ε . To this effect, we state the following lemma, whose proof is included in the Supplementary Material.

Lemma 3 Let \mathbb{P} be the original Potts measure given in (2), and let \mathbb{Q} be the low-rank Potts measure given in (6). Then we have the following results:

(i) The log normalizing constant between the two models satisfies

$$|\log Z(\beta, B_n) - \log Z(\beta, \tilde{B}_n)| \leq \frac{1}{2} n \beta \varepsilon.$$

(ii) With $KL(\cdot|\cdot)$ denoting the Kullback-Leibler divergence between two probability measures, we have

$$\max\left(KL(\mathbb{P}|\mathbb{Q}), KL(\mathbb{Q}|\mathbb{P})\right) \leq n \beta \varepsilon.$$

The low-rank Auxiliary Gaussian gives a parsimonious representation only if $k = \text{rank}(\tilde{B}_n) \ll n$. The following lemma provides a simple sufficient condition as to when this happens.

Lemma 4 Suppose λ_{\max} and λ_{\min} are the largest and smallest eigenvalues of A_n . Let $B_n := \beta(A_n + |\lambda_{\min}|I_n)$, and \tilde{B}_n be its low-rank approximation for some $\varepsilon > 0$. If

$$\lambda_{\max} = O(1), \quad \lambda_{\min} = o(1), \quad (11)$$

then $k_n := \text{rank}(\tilde{B}_n) = o(n)$.

The proof of this lemma is included in the Supplementary Material.

The above lemma raises the question of whether there are natural examples of matrices A_n which satisfy (11). Below we give some examples of matrices A_n which satisfy (11), and some examples which don't.

- **Satisfies** (11): Ising model on the Complete Graph (Curie-Weiss model), Random regular graphs and Erdős-Rényi graphs with large average degree, Hopfield model with $m \ll n$.
- **Does not satisfy** (11): Ising model on graphs with bounded average (including Ising model on the integer lattice), Hopfield model with $m = n$, SK model.

If (11) is not satisfied, then it seems reasonable to prefer the regular version of the Auxiliary Gaussian algorithm over the low-rank version. Numerical experiments suggest the regular version is slightly faster when A_n is full-rank.

3 Numerical experiments

We now study the performance of various MCMC samplers on a range of Potts models.

When A_n is the scaled adjacency matrix of a graph G_n , the state of the art algorithms are based on constructing auxiliary clusters, which form a random partition of the vertices of the nodes of G_n . Once an auxiliary cluster has been constructed, all the nodes in one cluster are now assigned a common new spin value according to some probability. Thus potentially many states can be updated at once, which allows for a fast exploration of the sample space. The most well known examples in this class are the Swendsen-Wang and Wolff algorithms [Swendsen and Wang, 1987, Wolff, 1989]. We find in our experiments that the Wolff algorithm is more efficient than Swendsen-Wang, a result consistent with the Physics literature [e.g Wolff, 1989, Landau and Binder, 2009]. For this reason, we only report comparison of our Auxiliary Gaussian algorithms (both the original and the low-rank version) with the Wolff algorithm. In the Supplementary Material, we offer a brief review of auxiliary cluster algorithms. Another algorithm we use to compare our results is the classic Heat Bath algorithm.

For the spin glass models we no longer have access to auxiliary cluster algorithms. In this case we only use the Heat Bath algorithm as the benchmark, and compare it with our proposed Auxiliary Gaussian (AG) samplers. In the special case of the Ising model where

$q = 2$, we use a specialized AG algorithm which reduces the dimension of the auxiliary Gaussian variables from $2n$ to n ($2k$ to k when doing a low-rank approximation) which improves the performance of the AG sampler (see Supplementary Material for details on this specialized version of the algorithm for $q = 2$). The non low-rank specialization reduces to the auxiliary Gaussian variable based algorithm introduced by Martens and Sutskever [2010]. All samplers are implemented in R using the same packages to attempt a fair comparison. As we explain below, the utility of each method depends heavily on the coupling matrix A_n , and the inverse temperature β .

3.1 Performance metrics

Our goal is to construct Monte Carlo estimators for $\mathbb{E}_{\mathbb{P}}\phi(\mathbf{X})$, where $\phi : [q]^n \rightarrow \mathbb{R}$, via the sample average

$$\delta_m = \sum_{i=1}^m \phi(\mathbf{x}^{(i)}) / m.$$

Here $\{\mathbf{x}^{(1)}, \dots, \mathbf{x}^{(m)}\}$ represent the output of the first m iterations of the MCMC algorithm. If $\text{Var}_{\mathbb{P}}\phi(X) < \infty$ and the samples are i.i.d., δ_m is unbiased, and has variance $\text{Var}(\delta_m) = \text{Var}_{\mathbb{P}}\phi(X)/m$. Unfortunately the samples we generate with MCMC are approximate: they are not independent and, for a finite number of iterations of our MCMC algorithm, they are biased. Practitioners typically expect that, after a certain number of iterations, the Markov chain converges to a stationary distribution and is unbiased. The first samples are discarded, thereby removing the initial bias of the so-called ‘‘burn in’’ phase. However, depending on the inverse-temperature parameter β (and in particular for large β), MCMC algorithms for Ising and Potts models can be notoriously slow to mix: even after many iterations, they may fail to overcome the initial transient bias. One way to diagnose MCMC convergence is to run multiple chains with different initializations, and check that they produce Monte Carlo estimators in good agreement. We perform such a check with the rank-normalized \hat{R} statistics developed by Vehtari et al. [2020], which estimates ratio of the variance across all chains over the variance within each chain. If the chains are mixing, \hat{R} should be close to 1, and eventually it should converge to 1 as the number of iterations converges to $+\infty$. Another sanity check is to confirm that Monte Carlo estimators produced by different algorithms are in agreement with one another.

Once we trust our estimator to be unbiased, we examine the *effective sample size*, defined by

$$m_{\text{eff}} = \frac{\text{Var}\phi(X)}{\text{Var}(\delta_m)}.$$

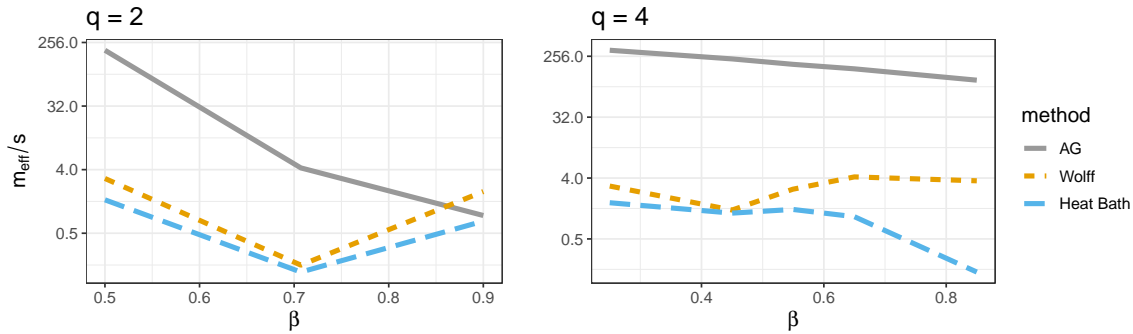


Figure 1: Effective sample size per second for grid model.

If the samples are independent, then $m_{\text{eff}} = m$. MCMC typically generates correlated samples, which incurs a loss of information, in which case $m_{\text{eff}} < m$. A popular method for computing m_{eff} is via an autocorrelation function [c.f. Geyer, 2012]. We compute \hat{R} and m_{eff} using the R package Posterior [Gabry et al., 2021].

Our performance metric is the effective sample size per second, m_{eff}/s . The effective sample size alone considers how well the MCMC algorithm mixes over iterations but it does not consider the computation cost of each iteration. A useful sampler finds a good balance between computing iterations quickly, and generating samples with a low autocorrelation. We focus on the summary function $\phi(\mathbf{x}) = \beta \sum_{i,j=1}^n A_n(i,j) 1\{x_i = x_j\}$, which is the system’s Hamiltonian.

3.2 Potts models on a graph

We begin with the case where A_n is the adjacency matrix of a graph G_n scaled by its average degree. We consider two choices of G_n which are of wide interest in Statistical Physics: the Ising model on the integer lattice and the Curie-Weiss model. For the subsequent experiments in this section, we run 4 chains each for $m = 10,000$ iterations, and discard the first 1,000 iterations of each chain as burn-in.

Lattice graph. The two-dimensional lattice graph $[1, \sqrt{n}]^2$ with two states (i.e. $q = 2$) is possibly the most well-studied example. We examine a 16×16 graph (i.e. $n = 256$), and consider the cases $q = 2, 4$. We focus on a parameter range in β around the critical temperature $\beta_c(q)$, which is approximately 0.44 and 0.55 for $q = 2$ and $q = 4$ respectively, as reported in Monroe [2002]. Overall the AG sampler offers the best performance, as measured by m_{eff}/s (Figure 1). We note, however, a very sharp drop in performance of the AG algorithm as β increases beyond criticality, for $q = 2$. In comparison, for $q = 4$ our algorithm performs much bet-

ter at or beyond criticality. This may be because the larger sample space allows for more exploration, and as such decreases autocorrelation between updates. In the case $q = 2$, the Wolff sampler, by contrast, is more robust to large β ; we believe this is because at cold temperatures the coupling between nodes is stronger, allowing the Wolff algorithm to construct large auxiliary clusters and update more nodes at once. These global updates lead to a decrease in autocorrelation. The expected slow down at critical temperature for $q = 2$ is apparent for all the three samplers.

Curie-Weiss model. In this model $A_n = \frac{1}{n} \mathbf{1}\mathbf{1}' - \frac{1}{n} I_n$ is the scaled adjacency matrix of a complete graph, where each node is connected to every other node. We once again consider the cases $q = 2, 4$, with $n = 256$. The critical value $\beta_c(q)$ is 1 and ~ 1.64 for $q = 2$ and $q = 4$ respectively [e.g. Bollobás et al., 1996], around which we focus our simulations. Adjusting the diagonal elements, we obtain a rank-1 coupling matrix on which we can apply the low-rank AG sampler. The same update rule is obtained by truncating the spectral expansion of B_n , using the threshold $\varepsilon = 10^{-12}$ which is slightly above machine precision, as our tolerance for eigenvalues. Figure 2 shows the performance measurements. In the Ising case (i.e. $q = 2$), the AG samplers offer the best performance by several orders of magnitude. The low-rank sampler offers a $\sim 3 - 4$ fold speed up over the regular AG sampler. The story is quite different at $q = 4$. As we near the value $\beta = 1.65$, we observe a sharp drop in efficiency for the Heat Bath and the AG samplers. For $\beta > 1.65$, the chains fail to mix, as notably indicated by the \hat{R} statistic, and produce wildly inaccurate estimates of $\mathbb{E}\phi(\mathbf{X})$. A previous study found that the Heat Bath undergoes a dramatic slow down near $\beta \approx 1.65$ [Cuff et al., 2012]. Clearly this behavior also affects the AG samplers. The Wolff and Swendsen-Wang algorithms are by contrast not affected by this phenomenon, and produce accurate Monte Carlo estimates for $\beta > 1.65$.

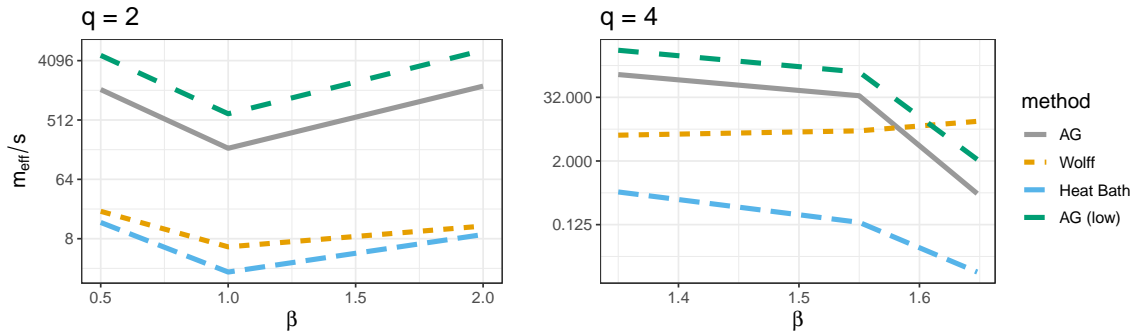


Figure 2: Effective sample size per second for Curie-Weiss model.

3.3 Spin Glass Potts models

In a Spin Glass model, the entries in A_n can take both positive and negative values. Two important examples are the Hopfield model and the Sherrington-Kirkpatrick (SK) models. For these problems, the Wolff and Swendsen-Wang algorithms are no longer an option.

Hopfield model. As before, we run 4 chains each with $m = 10,000$ sampling iterations, discarding the first 1,000 samples as a burn-in phase. Let $\eta \in \mathbb{R}^{d \times n}$ be a matrix of i.i.d random variables with $P(\eta_{ik} = \pm 1) = 1/2$, and let

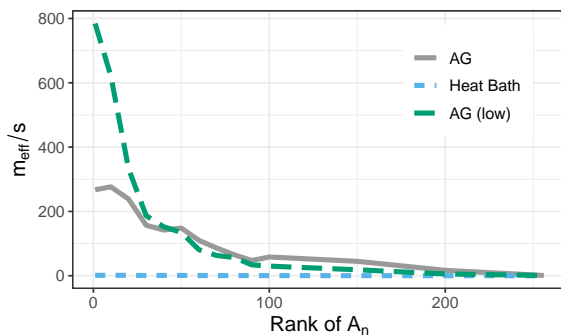
$$A_n = \max(n, d)^{-1} \eta' \eta. \quad (12)$$

By convention we should zero out the diagonals of A_n . But since changing diagonal entries does not impact the distribution, and (12) is the commonly specified form of the Hopfield matrix, we will use (12). Now A_n can take values which are positive, negative, or zero, meaning the spins X_i can be correlated, anti-correlated, or uncorrelated. It is usually not possible to set each node to be equal, so as to maximize $A_n(i, j)1\{x_i = x_j\}$ for all (i, j) , as a result of which the emergent system is said to be frustrated.

In this case, if $d \ll n$, then standard concentration results show that $A_n = n^{-1} \eta' \eta \approx I_n$, which has all positive eigenvalues. Thus for $d \ll n$, all eigenvalues of $A_n - \text{diag}(A_n)$ should be close to 0 with high probability. Consequently, (11) will hold, and so the low-rank algorithm should be used. As d increases, the low-rank algorithm should become worse, until it becomes comparable to (or slightly worse than) the regular AG algorithm. We use this example to examine the validity of the above prediction, and to compare the regular and the low-rank AG samplers across varying ranks. We set $\beta = 1$, $q = 4$, $n = 256$, and vary d from 1 to 100. Setting $\varepsilon = 10^{-12}$, as we did with the Curie-Weiss model, we find the low-rank AG incorrectly treats A_n as full-rank. This is due to the numerical errors that

arise when computing eigenvalues. Setting $\varepsilon = 10^{-10}$ fixes the issue for this particular problem. Overall the AG samplers offer performance which is two orders of magnitude faster than the Heat Bath. The low-rank AG offers the best performance for small d , but this advantage vanishes as the rank of A_n increases (Figure 3).

Remark 5 *In all our experiments, the regular and low-rank AG generate roughly the same effective sample size. The difference in performance is therefore driven by the difference in the computational cost of each iteration.*


 Figure 3: Effective sample size per second for Hopfield Potts model with $q = 4$ and $\beta = 1$.

Cold SK model. In the SK model, the elements of a coupling matrix $\{A_n(i, j)\}_{1 \leq i < j \leq n}$ are mutually independent, drawn from a standard normal scaled by $1/\sqrt{n}$, equivalently a normal with variance $1/n$:

$$A_n(i, j) = A_n(j, i) \sim \text{Normal}(0, n^{-1}).$$

This coupling matrix unfortunately does not admit a good low-rank approximation (c.f. Basak and Mukherjee [2017]). An important application of this model in Physics is the study of spin glass systems at cold temperatures, i.e. below the critical temperature [e.g

Katzgraber et al., 2001, Yucesoy, 2013]. We have seen in our previous experiments that the performance of the Heat Bath and the AG sampler suffers as β increases. This is also true for the SK model. For high β , the Potts model becomes highly multimodal, resulting in a slow or incomplete exploration by the Markov chains.

Tempering algorithms can mitigate this problem and be coupled with any sampling scheme. The tempered Heat Bath is a popular method to draw samples from cold Spin Glass models [e.g Swendsen and Wang, 1986, Hukushima et al., 1998]. As we shall see, this strategy is further enhanced when we replace the Heat Bath with an AG sampler (Figure 4). A tempering algorithm runs multiple chains or *replicas* over a sequence of temperatures for a set number of iterations and then exchanges, with a certain probability, the states of two replicas with a neighboring temperature. The probability of exchanging two neighboring replicas is chosen so as to maintain detailed balance. At high temperatures, the Markov chain can move more easily across the target space and overcome the energy barriers between modes, before being cooled down again to sample at the temperature of interest. Naturally we can run replicas in parallel.

When implementing a tempering algorithm, we need to choose the number of replicas and their respective temperatures. The first replica is at the cold temperature of interest. We then progressively increase the temperature of each replica to insure that the exchange probability is high, and that we eventually reach a warm temperature at which the sampler is not frustrated by high energy barriers. Additional details about the tempering algorithm can be found in the Supplementary Material.

In our experiment, the target inverse-temperature is $\beta = 3$, which is way above the critical parameter. We create 11 replicas with $\beta = (0.5, 0.75, 1, 1.25, 1.5, 1.75, 2, 2.25, 2.5, 2.75, 3)$. We find this yields reasonable, if somewhat uneven, acceptance rates for the exchange proposals. A more principled approach to setting temperatures is described by Hukushima et al. [1998]. In total, we attempt 40 exchanges and run 1,000 iterations between exchanges, for a total of 40,000 iterations. As before, we run 4 chains – or here 4 sets of replicas – with different initializations to compute \hat{R} and monitor whether the chains are mixing. The size of the system is $n = 128$.

Figure 4 presents the results of our experiment. We measure the efficiency of a tempered AG sampler, a tempered Heat Bath, and a regular AG sampler. The non-tempered AG suffers at colder temperatures and for $\beta > 2.5$, AG produces Monte Carlo estimates in

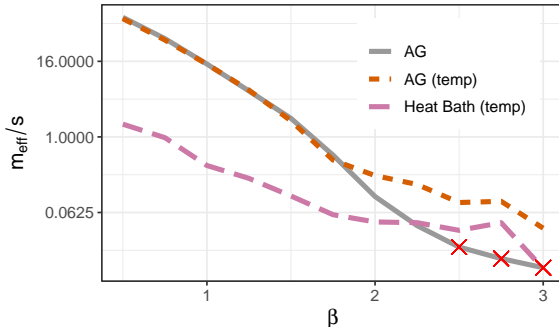


Figure 4: Effective sample size per second for SK Potts model. For $\beta \geq 2.5$, the AG sampler, without tempering, returns estimates in disagreement with the other samplers and has poor \hat{R} diagnostics. The measured effective sample size at these temperatures for the AG sampler should not be trusted, as indicated by an “x”.

disagreement with competing algorithms; furthermore the large \hat{R} values ($\hat{R} > 1.2$) suggest the Markov chains are not mixing. The tempered AG offers the best performance across all temperatures. We note that at $\beta = 3$, for both tempered algorithms, $\hat{R} \approx 1.13$, which suggests we at least ought to run more iterations to produce more accurate estimates. Finally while tempering offers significant improvement, the sharp drop in performance with increasing β is still present.

4 Discussion

AG samplers offer a competitive and at times largely superior performance across a range of models, particularly in high temperature regimes and at criticality. There are some exceptions to this in the low temperature regime, such as the Ising model on the 2D lattice ($q = 2$), and the Curie-Weiss Potts models with $q = 4$. Similar to the Heat Bath algorithm, the AG algorithms are sensitive to the system’s temperature, and tempering can alleviate this issue. Examining the alternative algorithms (cluster algorithms and the Heat Bath), we find there is no universal algorithm that efficiently handles all the pathologies we may encounter when dealing with Ising and Potts models for various coupling matrices across different choices of q . Care must be taken when picking a sampler.

Various operations in Algorithm 1 can be parallelized to further improve performance. This observation also holds for the low-rank AG sampler, and gradient-based samplers that target the marginal distribution of \mathbf{Z} . As such, Auxiliary Gaussian methods are amiable to use on accelerators such as GPUs. We remind readers that high-performance computing should be used responsibly, given its energy consumption.

5 Acknowledgment

The second author gratefully thanks NSF (DMS-1712037, DMS-2113414) for support during this research.

References

- A. Basak and S. Mukherjee. Universality of the mean-field for the potts model. *Probability Theory and Related Fields*, 168:557 – 600, 2017.
- B. Bollobás, G. Grimmett, and S. Janson. The random-cluster model on the complete graph. *Probability Theory and Related Fields*, 104:283 – 317, 1996.
- P. Cuff, J. Ding, O. Louidor, E. Lubetzky, Y. Peres, and A. Sly. Glauber dynamics for the mean-field potts model. *Journal of Statistical Physics*, 149:432 – 477, 2012.
- A. M. Ferrenberg, J. Xu, and D. P. Landau. Pushing the limits of monte carlo simulations for the 3d ising model. *Physical Review E*, 97, 2018. doi: 10.1103/PhysRevE.97.043301.
- J. Gabry, P. Buekner, and M. Kay. posterior. 2021. URL <https://github.com/jgabry/posterior>.
- C. Geyer. *Introduction to Markov Chain Monte Carlo*. Brooks, Steve and Gelman, Andrew and Jones, Galin L and Meng, Xiao-Li, 2012.
- W. Grathwohl, K. Swersky, M. Hashemi, D. Duvenaud, and C. J. Maddison. Oops i took a gradient: Scalable sampling for discrete distributions. *Proceedings of the 2021 International Conference on Machine Learning*, 2021.
- K. Hukushima and K. Nemeto. Exchange monte carlo method and application to spin glass simulations. *Journal of the Physical Society of Japan*, 65:1604 – 1608, 1996.
- K. Hukushima, H. Takajama, and H. Yoshina. Exchange monte carlo dynamics in the sk model. *Journal of the Physical Society of Japan*, 67:12 – 15, 1998.
- E. Ising. Beitrag zur theorie des ferromagnetismus. *Zeitschrift für Physik*, 31, 1925.
- H. G. Katzgraber, M. Palassini, and A. P. Young. Monte carlo simulations of spin glasses at low temperatures. *Physical Review B*, 63, 2001.
- D. Landau and K. Binder. *A Guide to Monte Carlo Simulations in Statistical Physics*. CAMBRIDGE UNIVERSITY PRESS, 2009.
- J. Martens and I. Sutskever. Parallelizable sampling of markov random fields. *Proceedings of the 13th International Conference on Artificial Intelligence and Statistics (AISTATS)*, 9, 2010.
- J. L. Monroe. Critical temperature estimates for higher-spin ising and potts models. *Physical Review*, 66, 2002.
- R. Mukherjee, S. Mukherjee, and M. Yuan. Global testing against sparse alternatives under ising models. *Annals of Statistics*, 46, 2018. doi: 10.1214/17-AOS1612.
- S. Mukherjee and Y. Xu. Statistics of the two-star ergm. *arXiv:1310.4526*, 2021.
- R. M. Neal. Probabilistic inference using markov chain monte carlo methods. *Technical Report CRG-TR-93-1*, 1993.
- R. B. Potts. Some generalized order-disorder transformations. *Mathematical Proceedings*, 48:106 – 109, 1952. doi: doi:10.1017/S0305004100027419.
- R. Swendsen and J.-S. Wang. Replica monte carlo simulation of spin-glasses. *Physical Review letters*, 57, 1986.
- R. H. Swendsen and J.-S. Wang. Nonuniversal critical dynamics in monte carlo simulations. *Physics review letter*, 58, 1987.
- A. Vehtari, A. Gelman, D. Simpson, B. Carpenter, and P.-C. Bürkner. Rank-normalization, folding, and localization: An improved \hat{r} for assessing convergence of mcmc. *Bayesian analysis*, 2020. doi: doi:10.1214/20-BA1221.
- U. Wolff. Collective monte carlo updating for spin systems. *Physical review journal*, 62, 1989. doi: doi: 10.1103/PhysRevLett.62.36.
- B. Yucesoy. *Replica Exchange Monte Carlo Simulations of the Ising Spin Glass: Static and Dynamic Properties*, volume 832. 2013. doi: <https://doi.org/10.7275/zqm3-ew06>.
- Y. Zhang, C. Sutton, A. Storkey, and Z. Ghahramani. Continuous relaxations for discrete hamiltonian monte carlo. *Advances in Neural Information Processing Systems 25*, 2012.

Appendix

The Appendix contains proofs missing in the main body. We derive the conditional and marginal distributions, that arise when we introduce either a regular or low-rank auxiliary Gaussian variable for Potts models. We prove Lemma 3, which characterizes the error committed in using the low-rank algorithm, and Lemma 4, which characterizes the type of coupling matrices for which we may want to use a low-rank algorithm. Specialized algorithms for the Ising model ($q = 2$) are derived. We also provide an overview on auxiliary cluster and tempering algorithms.

The code used for our numerical experiments can be found at https://github.com/charlesm93/potts_simulation. The ReadMe provides instructions on how to run the code.

A Missing proofs

A.1 Conditional and marginal distributions when using the regular Auxiliary Gaussian

We begin by proving Equations (4) and (5). Recall from (2) that the marginal p.m.f. of \mathbf{X} under \mathbb{P} is proportional to

$$\exp\left(\frac{1}{2} \sum_{\ell=1}^q \mathbf{y}'_{\ell} B_n \mathbf{y}_{\ell}\right).$$

Also from (3), the conditional density of \mathbf{Z} given $\mathbf{X} = \mathbf{x}$ is proportional to

$$\exp\left(-\frac{1}{2} \sum_{\ell=1}^q (\mathbf{z}_{\ell} - \mathbf{y}_{\ell})' B_n (\mathbf{z}_{\ell} - \mathbf{y}_{\ell})\right).$$

Thus, the joint distribution of \mathbf{X} and \mathbf{Z} is proportional to

$$\begin{aligned} & \exp\left(\frac{1}{2} \sum_{\ell=1}^q \left[\mathbf{y}'_{\ell} B_n \mathbf{y}_{\ell} - (\mathbf{z}_{\ell} - \mathbf{y}_{\ell})' B_n (\mathbf{z}_{\ell} - \mathbf{y}_{\ell})\right]\right) \\ &= \exp\left(-\frac{1}{2} \sum_{\ell=1}^q \mathbf{z}'_{\ell} B_n \mathbf{z}_{\ell} + \sum_{\ell=1}^q \mathbf{z}'_{\ell} B_n \mathbf{y}_{\ell}\right) \\ &= \exp\left(-\frac{1}{2} \sum_{\ell=1}^q \mathbf{z}'_{\ell} B_n \mathbf{z}_{\ell} + \sum_{\ell=1}^q \sum_{i=1}^n \sum_{j=1}^n z_{\ell}(j) B_n(i, j) 1\{x_i = \ell\}\right). \end{aligned} \quad (13)$$

From (13), we see that given \mathbf{Z} , the random variables (X_1, \dots, X_n) are mutually, independent, with

$$\mathbb{P}(X_i = \ell | \mathbf{Z}) \propto \exp\left(\sum_{j=1}^n B_n(i, j) z_{\ell}(j)\right),$$

which verifies (4).

The marginal distribution of \mathbf{Z} is obtained from (13) by summing over $\mathbf{x} \in [q]^n$, from which (5) follows.

A.2 Conditional and marginal distributions when using the low-rank Auxiliary Gaussian

Next we prove Equations (8) and (10). Recall from (7) that the marginal p.m.f. of \mathbf{X} under \mathbb{P} is proportional to

$$\exp\left(\frac{1}{2} \sum_{\ell=1}^q \sum_{j=1}^k \mu_j (\mathbf{p}'_j \mathbf{y}_{\ell})^2\right).$$

Also from (9), the conditional density of \mathbf{Z} given $\mathbf{X} = \mathbf{x}$ is proportional to

$$\exp\left(-\frac{1}{2} \sum_{\ell=1}^q \sum_{j=1}^k \mu_j (z_{\ell}(j) - \mathbf{p}'_j \mathbf{y}_{\ell})^2\right).$$

Thus, the joint distribution of \mathbf{X} and \mathbf{Z} is proportional to

$$\begin{aligned}
 & \exp\left(\frac{1}{2}\sum_{\ell=1}^q\sum_{j=1}^k\mu_j\left[\left(\mathbf{p}'_j\mathbf{y}_\ell\right)^2-\left(z_\ell(j)-\mathbf{p}'_j\mathbf{y}_\ell\right)^2\right]\right) \\
 &= \exp\left(-\frac{1}{2}\sum_{\ell=1}^q\sum_{j=1}^k\mu_j z_\ell(j)^2+\sum_{\ell=1}^q\sum_{j=1}^k\mu_j z_\ell(j)\mathbf{p}'_j\mathbf{y}_\ell\right) \\
 &= \exp\left(-\frac{1}{2}\sum_{\ell=1}^q\sum_{j=1}^k\mu_j z_\ell(j)^2+\sum_{\ell=1}^q\sum_{j=1}^k\sum_{i=1}^n\mu_j z_\ell(j)p_j(i)1\{x_i=\ell\}\right). \tag{14}
 \end{aligned}$$

Using (14), given $\mathbf{Z} = \mathbf{z}$ the random variables (X_1, \dots, X_n) are mutually, independent, with

$$\mathbb{P}(X_i = \ell | \mathbf{Z}) \propto \exp\left(\sum_{j=1}^k\mu_j z_\ell(j)p_j(i)\right),$$

which verifies (9). The marginal distribution of \mathbf{Z} is obtained from (14) by summing over $\mathbf{x} \in [q]^n$, from which (10) follows.

A.3 Proof of Lemma 3

With B_n and \tilde{B}_n as in the Hamiltonians of the distributions \mathbb{P} and \mathbb{Q} in (2) and (6) respectively, for any $\mathbf{x} \in [q]^n$, we have

$$\begin{aligned}
 \left|\sum_{i,j=1}^n B_n(i,j)1\{x_i=x_j\}-\sum_{i,j=1}^n \tilde{B}_n(i,j)1\{x_i=x_j\}\right| &= \left|\sum_{\ell=1}^q \mathbf{y}'_\ell(B_n-\tilde{B}_n)\mathbf{y}_\ell\right| \\
 &\leq \sum_{\ell=1}^q \|\mathbf{y}_\ell\|_2^2 \|B_n-\tilde{B}_n\|_2 \\
 &= \|B_n-\tilde{B}_n\|_2 \sum_{\ell=1}^q \sum_{i=1}^n 1\{x_i=\ell\} \tag{15}
 \end{aligned}$$

$$= n \|B_n-\tilde{B}_n\|_2 \leq n\varepsilon. \tag{16}$$

where the last bound uses the definition of \tilde{B}_n to note that all eigenvalues of $B_n-\tilde{B}_n$ are smaller than ε in absolute value. Thus, for any $\mathbf{x} \in [q]^n$, we have

$$e^{-\frac{n\beta\varepsilon}{2}} \leq \frac{\exp\left(\frac{\beta}{2}\sum_{i,j=1}^n B_n(i,j)1\{x_i=x_j\}\right)}{\exp\left(\frac{\beta}{2}\sum_{i,j=1}^n \tilde{B}_n(i,j)1\{x_i=x_j\}\right)} \leq e^{\frac{n\beta\varepsilon}{2}}. \tag{17}$$

On summing over $\mathbf{x} \in [q]^n$, this gives

$$e^{-\frac{n\beta\varepsilon}{2}} \leq \frac{Z(\beta, A_n)}{Z(\beta, \tilde{A}_n)} \leq e^{\frac{n\beta\varepsilon}{2}}, \tag{18}$$

which verifies part (i). For verifying part (ii), taking a ratio of (17) and (18) we get

$$e^{-n\beta\varepsilon} \leq \frac{\mathbb{P}(\mathbf{X}=\mathbf{x})}{\mathbb{Q}(\mathbf{X}=\mathbf{x})} \leq e^{n\beta\varepsilon},$$

which gives $\max(\text{KL}(\mathbb{P}|\mathbb{Q}), \text{KL}(\mathbb{Q}|\mathbb{P})) \leq n\beta\varepsilon$. This verifies part (ii), and hence completes the proof of the lemma.

A.4 Proof of Lemma 4

To begin, we bound k by examining the trace of B_n^2 , and noting that, per Markov's inequality,

$$k \leq \sum_{i=1}^n \mu_i^2 / \varepsilon^2 = \text{tr}(B_n^2) / \varepsilon^2.$$

Also, we have

$$\text{tr}(B_n^2) = \text{tr}(A_n^2 + 2\lambda_{\min}A_n + \lambda_{\min}^2 I_n) = \text{tr}(A_n^2) + n\lambda_{\min}^2. \quad (19)$$

Combining the above two displays, it suffices to show that the RHS of (19) is $o(n)$. Since $\lambda_{\min} = o(1)$, it suffices to show $\text{tr}(A_n^2) = o(n)$, which is the focus of the rest of the proof.

To this effect, recall that $\text{tr}(A_n) = 0$. Thus, with $\lambda_1(A_n), \dots, \lambda_n(A_n)$ denoting the eigenvalues of A_n we have

$$\sum_{i=1}^n \lambda_i(A_n) 1\{\lambda_i(A_n) > 0\} = \sum_{i=1}^n |\lambda_i(A_n)| 1\{\lambda_i(A_n) < 0\} \leq n|\lambda_{\min}|.$$

This in turn gives

$$\sum_{i=1}^n |\lambda_i(A_n)| = \sum_{i=1}^n \lambda_i(A_n) 1\{\lambda_i(A_n) > 0\} + \sum_{i=1}^n |\lambda_i(A_n)| 1\{\lambda_i(A_n) < 0\} \leq 2n|\lambda_{\min}| = o(n),$$

and so

$$\text{tr}(A_n^2) = \sum_{i=1}^n \lambda_i(A_n)^2 \leq \lambda_{\max} \sum_{i=1}^n |\lambda_i(A_n)| = o(n),$$

where the last equality uses the assumption $\lambda_{\max} = O(1)$. This completes the proof of the lemma.

B Specialized Auxiliary Gaussian algorithm for $q = 2$

B.1 Standard Auxiliary Gaussian algorithm

Setting $\mathbf{W} := \mathbf{Z}_1 - \mathbf{Z}_2$ and using (3), under \mathbb{P} we have

$$(\mathbf{W} | \mathbf{X} = \mathbf{x}) \sim N(\mathbf{y}_1 - \mathbf{y}_2, 2B_n^{-1}). \quad (20)$$

Also, using (4), we have

$$\begin{aligned} \mathbb{P}(X_i = 1 | \mathbf{Z} = \mathbf{z}) &= \frac{\exp\left(\sum_{j=1}^n B_n(i, j) z_1(j)\right)}{\exp\left(\sum_{j=1}^n B_n(i, j) z_1(j)\right) + \exp\left(\sum_{j=1}^n B_n(i, j) z_2(j)\right)} \\ &= \frac{\exp\left(\frac{1}{2} \sum_{j=1}^n B_n(i, j) w(j)\right)}{\exp\left(\frac{1}{2} \sum_{j=1}^n B_n(i, j) w(j)\right) + \exp\left(-\frac{1}{2} \sum_{j=1}^n B_n(i, j) w(j)\right)}, \end{aligned} \quad (21)$$

where $w_j = z_1(j) - z_2(j)$. A similar calculation gives

$$\mathbb{P}(X_i = 2 | \mathbf{Z} = \mathbf{z}) = \frac{\exp\left(-\frac{1}{2} \sum_{j=1}^n B_n(i, j) w(j)\right)}{\exp\left(\frac{1}{2} \sum_{j=1}^n B_n(i, j) w(j)\right) + \exp\left(-\frac{1}{2} \sum_{j=1}^n B_n(i, j) w(j)\right)}.$$

Thus, instead of using the $2n$ dimensional Gaussian \mathbf{Z} , one can use the n dimensional Gaussian W , and iterate between (20) and (21). This is the same exact algorithm, but we work with a lower dimensional representation of the auxiliary variable, which helps in faster computations. We note that this is the exact same algorithm as [Martens and Sutskever, 2010] in the Ising case.

B.2 Low rank Auxiliary Gaussian algorithm

Setting $\mathbf{W} := \mathbf{Z}_1 - \mathbf{Z}_2$ as before, using (8) under \mathbb{Q} we have

$$(\mathbf{W}_j | \mathbf{X} = \mathbf{x}) \sim N(\mathbf{p}'_j(\mathbf{y}_1 - \mathbf{y}_2), 2/\mu_j), \quad (22)$$

with (W_1, \dots, W_k) mutually independent. Also, using (9), we have

$$\begin{aligned} \mathbb{Q}(X_i = 1 | \mathbf{Z} = \mathbf{z}) &= \frac{\exp\left(\sum_{j=1}^k \mu_j z_1(j) p_j(i)\right)}{\exp\left(\sum_{j=1}^k \mu_j z_1(j) p_j(i)\right) + \exp\left(\sum_{j=1}^k \mu_j z_2(j) p_j(i)\right)} \\ &= \frac{\exp\left(\frac{1}{2} \sum_{j=1}^k \mu_j w_j p_j(i)\right)}{\exp\left(\frac{1}{2} \sum_{j=1}^k \mu_j w_j p_j(i)\right) + \exp\left(-\sum_{j=1}^k \mu_j w_j p_j(i)\right)}, \end{aligned} \quad (23)$$

where $w_j = z_1(j) - z_2(j)$. A similar calculation gives

$$\mathbb{Q}(X_i = 2 | \mathbf{Z} = \mathbf{z}) = \frac{\exp\left(-\frac{1}{2} \sum_{j=1}^k \mu_j w_j p_j(i)\right)}{\exp\left(\frac{1}{2} \sum_{j=1}^k \mu_j w_j p_j(i)\right) + \exp\left(-\sum_{j=1}^k \mu_j w_j p_j(i)\right)}.$$

Thus, instead of using the $2k$ dimensional Gaussian \mathbf{Z} , one can use the k dimensional Gaussian W , and iterate between (22) and (23).

C Overview of the Swendsen-Wang and Wolff algorithms

The Heat Bath updates one node, x_j , at a time, conditional on the distribution of the other nodes, \mathbf{x}_{-j} . As a result, it can take many iterations to meaningfully change \mathbf{x} and the produced samples are strongly correlated. The Swendsen-Wang algorithm attempts to address this issue by updating large clusters of particles at each iteration. This is done by introducing an auxiliary random graph, as illustrated in Figure 5. Below we provide a sketch of the algorithm:

1. Construct auxiliary clusters until every node belongs to a cluster, per the following steps:
 - (a) Start a cluster at a random node, x_i , which does not already belong to an auxiliary cluster (call this a *free* node).
 - (b) For each free neighbor x_j of x_i , i.e. such that $A_n(i, j) > 0$, if $x_i = x_j$, add x_j to the cluster with probability
$$p(\beta) = 1 - \exp(-2\beta A_n(i, j))$$
 - (c) Continue growing the cluster by repeating the above step for each added node. Once the cluster stops growing, start a new cluster at one of the free nodes.
2. Once all the nodes have been assigned to a cluster, randomly assign a new state in $[q]$ to each cluster, where each state has equal probability.

Remark a *The algorithm can be generalized to the case where the Potts model admits an exterior magnetic field, which favors certain states over the others, by adjusting the probability in step 1(b).*

The Wolff algorithm only constructs one auxiliary cluster per iteration, even if this means not every node is assigned to an auxiliary cluster. The motivation for this is to not waste computational time building small clusters, as we do once there are only a few free nodes left. Another change is that in the Ising case ($q = 2$), the Wolff algorithm always flips the state of the cluster, rather than assigning $\{-1, +1\}$ with equal probability.

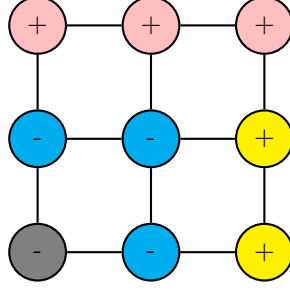


Figure 5: Color-coded random auxiliary clusters on a grid graph. In the Ising model ($q = 2$), each particle takes values in $\{-, +\}$, referring to the two states of the Ising model. The Swendsen-Wang algorithm randomly connects nodes in the same state to construct auxiliary clusters: here 4 auxiliary clusters are constructed (pink, blue, yellow, and gray).

D Overview of the tempering algorithm

A tempering algorithm runs multiple chains or *replicas* over a sequence of temperatures for a set number of iterations and then exchanges, with a certain probability, the states of two replicas with a neighboring temperature. The probability of exchanging two neighboring states, with inverse temperatures β_t and β_{t+1} , can be worked out from the detailed balance condition, following the argument by Hukushima and Nemoto [1996]. For convenience, we introduce the *partial Hamiltonian*

$$\mathcal{H}(A_n, \mathbf{x}_t) = -\frac{1}{2} \sum_{i,j=1}^n A_n(i,j) 1\{x_{t,i} = x_{t,j}\}$$

Assume $\beta_1 < \dots < \beta_t < \beta_{t+1} < \dots < \beta_T$. Consider the joint distribution over T replicas, $\{\mathbf{X}\} = \{\mathbf{X}_1, \mathbf{X}_2, \dots, \mathbf{X}_T\}$. The replicas are mutually independent, with joint p.m.f.

$$\mathbb{P}(\mathbf{X}_1 = \mathbf{x}_1, \dots, \mathbf{X}_T = \mathbf{x}_T) = \prod_{t=1}^T \frac{\exp\left(\frac{\beta_t}{2} \sum_{i,j} A_n(i,j) 1\{x_{t,i} = x_{t,j}\}\right)}{Z(\beta_t, A_n)} = \prod_{t=1}^T \frac{\exp(-\beta_t \mathcal{H}(A_n, \mathbf{x}_t))}{Z(\beta_t, A_n)}.$$

We now introduce the transition kernel, $\Gamma(\mathbf{X}_t, \beta_t \mid \mathbf{X}_{t+1}, \beta_{t+1})$, which is the probability of exchanging the t^{th} and $(t+1)^{\text{th}}$ replicas. The detailed balance equation is satisfied, if

$$\begin{aligned} & \mathbb{P}(\mathbf{X}_1 = \mathbf{x}_1, \dots, \mathbf{X}_t = \mathbf{x}_t, \mathbf{X}_{t+1} = \mathbf{x}_{t+1}, \dots, \mathbf{X}_T = \mathbf{x}_T) \Gamma(\mathbf{X}_t, \beta_t \mid \mathbf{X}_{t+1}, \beta_{t+1}) \\ &= \mathbb{P}(\mathbf{X}_1 = \mathbf{x}_1, \dots, \mathbf{X}_t = \mathbf{x}_{t+1}, \mathbf{X}_{t+1} = \mathbf{x}_t, \dots, \mathbf{X}_T = \mathbf{x}_T) \Gamma(\mathbf{X}_{t+1}, \beta_t \mid \mathbf{X}_t, \beta_{t+1}). \end{aligned}$$

Thus

$$\begin{aligned} \frac{\Gamma(\mathbf{X}_t, \beta_t \mid \mathbf{X}_{t+1}, \beta_{t+1})}{\Gamma(\mathbf{X}_{t+1}, \beta_t \mid \mathbf{X}_t, \beta_{t+1})} &= \frac{\exp(-\beta_t \mathcal{H}(A_n, \mathbf{x}_{t+1}) - \beta_{t+1} \mathcal{H}(A_n, \mathbf{x}_t))}{\exp(-\beta_t \mathcal{H}(A_n, \mathbf{x}_t) - \beta_{t+1} \mathcal{H}(A_n, \mathbf{x}_{t+1}))} \\ &= \exp((\beta_{t+1} - \beta_t)(\mathcal{H}(A_n, \mathbf{x}_{t+1}) - \mathcal{H}(A_n, \mathbf{x}_t))). \end{aligned}$$

From this we deduce a Metropolis update with acceptance probability

$$\begin{aligned} & \Gamma(\mathbf{X}_t, \beta_t \mid \mathbf{X}_{t+1}, \beta_{t+1}) \\ &= \min(1, \exp[(\beta_{t+1} - \beta_t)(\mathcal{H}(A_n, \mathbf{x}_{t+1}) - \mathcal{H}(A_n, \mathbf{x}_t)]) \\ &= \min\left(1, \exp\left[\frac{1}{2}(\beta_{t+1} - \beta_t) \left(-\sum_{i,j=1}^n A_n(i,j) 1\{x_{t+1,i} = x_{t+1,j}\} + \sum_{i,j=1}^n A_n(i,j) 1\{x_{t,i} = x_{t,j}\}\right)\right]\right). \end{aligned} \quad (24)$$

Algorithm 2 provides the pseudo-code for a practical implementation.

Notation for the algorithm

- $\beta = (\beta_1, \beta_2, \dots, \beta_T)$: an array containing the inverse temperature for each replica, where T is the number of replicas.
- $\mathbf{x}_t^{(i)}$: the i^{th} sample for t^{th} replica.
- n_{ex} : the number of exchange steps.
- n_{mc} : the number of sampling iterations between exchange steps. Hence the total number of generated samples is $n_{\text{ex}} \times n_{\text{mc}}$.
- γ : the sampler used between exchanges.

Algorithm 2 Tempering

```

1: input:  $(\mathbf{x}_1^{(0)}, \mathbf{x}_2^{(0)}, \dots, \mathbf{x}_T^{(0)})$ ,  $\beta$ ,  $n_{\text{ex}}$ ,  $n_{\text{mc}}$ ,  $\gamma$ 
2: for  $i \in \{1, \dots, n_{\text{ex}}\}$ 
3:   for  $t \in \{1, \dots, T\}$  draw  $\mathbf{x}_t^{[(i-1)n_{\text{mc}}+1]:[in_{\text{mc}}]}$  using  $\gamma$ .
4:   for  $t \in \{1, \dots, T-1\}$ 
5:      $\mathcal{H}(\mathbf{x}_t) = -0.5 \sum_{\ell=1}^q (\mathbf{y}_{\ell,t}^{(in_{\text{mc}})})' A_n (\mathbf{y}_{\ell,t}^{(in_{\text{mc}})})$ 
6:      $\mathcal{H}(\mathbf{x}_{t+1}) = -0.5 \sum_{\ell=1}^q (\mathbf{y}_{\ell,t+1}^{(in_{\text{mc}})})' A_n (\mathbf{y}_{\ell,t+1}^{(in_{\text{mc}})})$ 
7:      $\Delta = (\beta_{t+1} - \beta_t) (\mathcal{H}(\mathbf{x}_{t+1}) - \mathcal{H}(\mathbf{x}_t))$ 
8:     Draw  $u \sim \text{uniform}(0, 1)$ .
9:     if  $(u \leq \exp(\Delta))$  (check whether or not to exchange states)
10:       $\mathbf{x}_{\text{saved}} = \mathbf{x}_{t+1}^{(in_{\text{mc}})}$ 
11:       $\mathbf{x}_t^{in_{\text{mc}}} = \mathbf{x}_{t+1}^{(in_{\text{mc}})}$ 
12:       $\mathbf{x}_{t+1}^{in_{\text{mc}}} = \mathbf{x}_{\text{saved}}$ 
13:    end if
14:  end for
15: end for
16: return:  $\mathbf{x}_1^{(1)}, \dots, \mathbf{x}_1^{(n_{\text{ex}}n_{\text{mc}})}, \dots, \mathbf{x}_T^{(1)}, \dots, \mathbf{x}_T^{(n_{\text{ex}}n_{\text{mc}})}$ 

```

Remark b The for loop at line 3 of Algorithm 2 can be parallelized, since between exchanges, samples for the replicas are generated independently.

Remark c We can rewrite line 5 to avoid redundant computations of $\mathcal{H}(\mathbf{x}_t)$, and insure that only one Hamiltonian is evaluated per iteration of the **for** loop at line 4. This requires some careful book-keeping, which we omitted to make the algorithm more readable. The computational gain from this step is marginal.

Remark d One can in theory use a different sampler for different replicas, though preliminary tests suggest there are no benefits to doing this.

In our numerical experiment on Spin Glass models (Section 3.3), we use $n_{\text{ex}} = 40$ and $n_{\text{mc}} = 1000$. Our experiment does not parallelize replicas.